Study of a scintillation counter consisting of a pure CsI crystal and avalanche photodiodes

Yifan JIN

Department of Physics, Graduate School of Science,

the University of Tokyo

August 25th, 2015

Abstract

Belle II, as an upgrade of Belle, aims at searching for New Physics with 40 times higher luminosity. Fast pure CsI scintillation crystals (τ = 30 ns) have been proposed to cope with the high luminosity. Silicon avalanche photodiodes are considered as one of the upgrade options.

At the University of Tokyo, we studied a counter consisting of pure CsI crystal ($6 \times 6 \times 30$ cm^3) and avalanche photodiodes (Hamamatsu APD S8664-1010 and S8664-55). The shot noise, thermal noise and additional noise were measured under shaping time ranging from 20 nanoseconds to 500 nanoseconds respectively. The total equivalent noise charge (ENC) has been calculated and compared with the value measured experimentally. The ENC is suppressed at theoretical limit. The equivalent noise energy (ENE) of the counter with several APDs has also been measured with cosmic muons. Further studies on optical greases and wrapping materials have been carried out in order to enhance the light collection efficiency. Optimal scheme has been established. The application of wavelength shifting plates (WLS), containing nanostructured organosilicon luminophores, matching the scintillation spectrum of pure CsI and APD's quantum efficiency perfectly, increases the signal substantially, therefore the signal-to-noise ratio improves considerably.

We confirm that by using several APD's coupling to pure CsI scintillation crystal and innovative WLS, the required electronic noise of 0.5 MeV can be obtained.

Contents

Chapter 1

Introduction

Belle experiment operated at KEKB accelerator was the world's highest luminosity e^+e^- collider, investigating CP-violation effects in B meson decays. Belle II, as an upgrade of Belle, aims at searching for New Physics with 40 times higher luminosity, through precision measurements extending from $B^{0(\pm)}$ meson decays to $B_s^{(*)}$ meson decays, charm physics, τ lepton physics, Υ-spectroscopy and pure electroweak measurements.

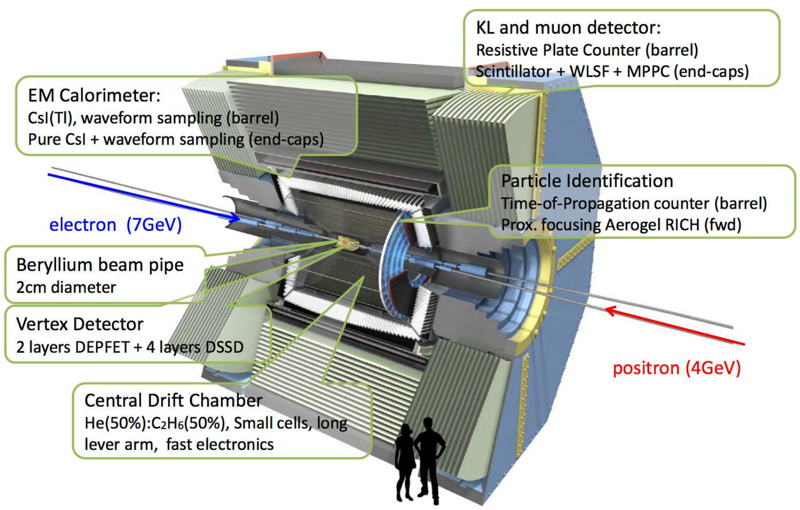

Figure 1.1: Belle II detector [1].

The electromagnetic calorimeter (ECL) is one of the most important parts of the Belle II detector, consisting of a 3 m long barrel section with an inner radius of 1.25 m and the annular endcaps at z = 2.0 m (forward part) and z = −1.0 m (backward part) from the interaction point. The calorimeter covers the polar angle region of $12.4° < \theta < 155.1°$, except two gaps ~ 1 ° wide between the barrel and endcaps.

In Belle, the pile up noise was not very notable. Now, as the luminosity will get increased by 40 times, the pile-up noise produced by the high rate low energy background photons will be very notable and severe, especially in end cap ECL. Therefore, the shaping time is set to be 30 ns for Belle II (in Belle, the shaping time was 1 μs). In this way, the pile-up noise can be reduced by a factor $\sqrt{\frac{\tau_{CsI(Tl)}=1\mu s}{\tau_{CsI(pure)}=30ns}} \approx 5.5$. As a result, fast pure CsI scintillation crystals with the scintillation decay time $\tau_{CsI} = 30$ ns for the ECL end caps have been proposed. Pure CsI crystals also own very good radiation hardness. Up to a γ irradiation dose of 10 krad, pure CsI crystals only shows a degradation of light yield less than 10% [1], which satisfies the requirement of Belle II. Unfortunately, the PIN-photodiodes, photosensors on CsI(Tl) crystals used in Belle, had been damaged by neutrons, resulting in a drastic increase on dark current. Meanwhile, taking into account the poor light yield of the pure CsI (one order smaller than that of CsI (Tl)), two options are considered for the photosensitive elements: vacuum photopentodes (PP) and silicon avalanche photodiodes (APD).

Vacuum photopentodes, recently developed by Hamamatsu Photonics, hold an extremely low capacitance of 10 pF. Such a 2-inch diameter device, has a quantum efficiency of about 15% at 310 nm and an internal gain of 120-200 under the condition without magnetic field. The electronics noise of PP is measured 30-40 keV without magnetic field. Taken into account the 1.5 T magnetic filed in Belle II and the stochastic noise, the expectation can be made around 200 keV [2]. However, asides from the excellent noise level of PP, due to the dimension of the device, only one PP is allowed to attach the crystal, which offers no redundancy. Thus, possibility of rendering a dead channel exists.

As a result, APD has also been proposed to be another candidate as a complementary approach. In this thesis, We investigate the second option with APD (Hamamatsu S8664-55 and S8664-1010). The advantages of APD are:

1. compactness, which allows several APDs to be attached to the crystal, providing redundancy in order to avoid an entirely dead channel; (no redundency in the case of photopentodes)

2. insensitivity to magnetic field; (the existence of magnetic induces the decrease on gain of photopentodes)

3. demanding of bias voltage only around 400 V; (over 800 V bias voltage is needed for photopentodes to work properly)

4. low dark current (at the order of $\sim$ nA) at the operating point (where gain of APD = 50), which diminishes the power dissipation of bias voltage supply.

Nevertheless, high equivalent noise charge (ENC), arising from short shaping time (30-50 ns) and large junction capacitance of APD (100-300 pF), along with the small light yield of pure CsI, results in a large equivalent noise energy (ENE). In the scheme with the actual size crystal ($6\times6\times30$ cm^3) and 1 APD (S8664-1010), ENE was measured to be about 2 MeV [1], which is 4 times the acceptable level ($\lesssim$ 0.5 MeV, see Appendix). The goal of my study is to reach the 0.5 MeV noise level.

In the following chapters, the electronics used in measurement are discussed in detail in Chapter 2. The measurement of equivalent noise charge is presented in Chapter 3, followed by the measurement of equivalent noise energy in Chapter 4. In order to reach the required noise level, further studies have been carried on, which is presented in chapter 5. Finally, conclusions and prospects are given in Chapter 6.

Chapter 2

Equipments in the experimental setup

In this chapter, the scheme of the measurement is illustrated, followed by the detailed specification of electronics modules in the readout electronic chain.

2.1 Scheme

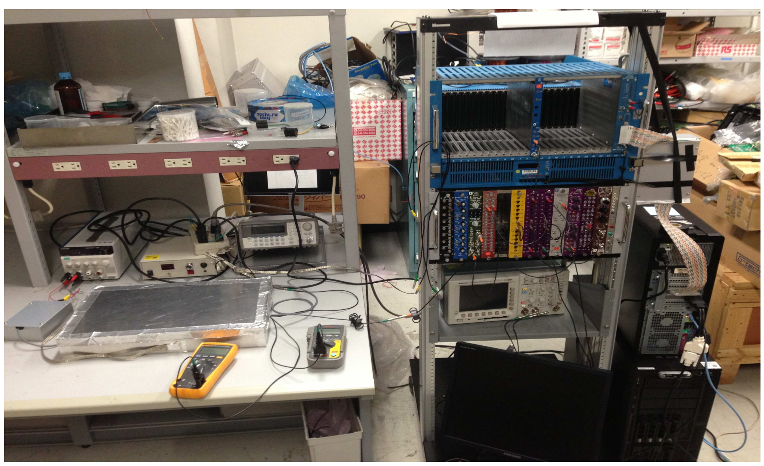

Figure 2.1: Photograph of the layout in the University of Tokyo.

In the University of Tokyo, the option with APD is studied here (see Fig.2.1). The scheme is sketched in Fig.2.2. A pure CsI crystal is wrapped by a layer of Gore-Tex teflon of 200 μm thickness and then covered by aluminized mylar film. The backward surface of the crystal is coupled with the Hamamatsu APD (S8664-1010 and S8664-55, see Fig.2.3) by optical grease OKEN 6262A. Then the signal is sent to the preamplifer as its amplitude is very tiny due to the poor light yield of pure CsI. After that, the signal gets processed by the shaping amplifier, read out by ADC and stored in the computer. At the same time, a discriminator, NTM-716, is used to send the gate signal to ADC, located

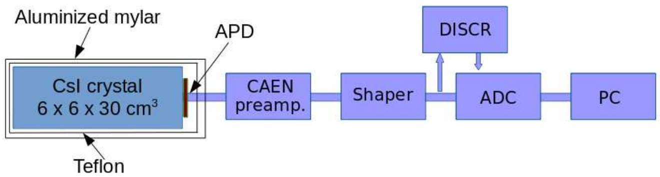

Figure 2.2: Scheme of the self-triggered measurement.

between shaper and ADC. The details of the APD, preamplifier, shaper and ADC are presented below. The specification of CsI crystal is in Chapter 4.

2.2 APD

Avalanche Photodiodes (APD) have been used in high energy physics for decades due to their merits such as high-speed response, high sensitivity, and ability to amplify a weak light signal into a large electrical signal.

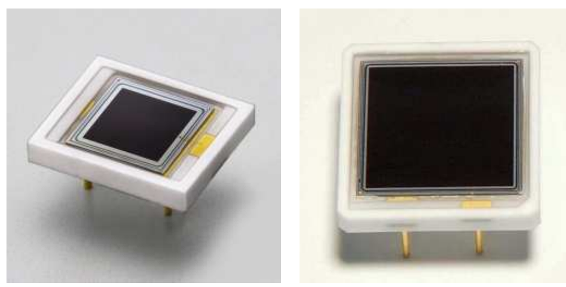

(a) S8664-55 (b) S8664-1010

Figure 2.3: Photograph of Hamamatsu APD[1].

The APD used in our counter system is HAMAMATSU Si APD S8664-55 and S8664-1010, of capacitances 80 pF and 270 pF and typical dark currents 3 nA and 10 nA respectively at the operating point (gain = 50). The active area 5 mm$\times$ 5 mm and 10 mm $\times$ 10 mm hold good uniformity at typical gain (g=50). The dimensions of these two APD, 10.6 mm $\times$ 9.0 mm and 13.7 mm $\times$ 14.5 mm (see Fig.2.4), provide the possibility of attaching 2 or 4 APD's per crystal.

Unfortunately, the quantum efficiency (QE) of Silicon APD (see Fig. 2.5) is not satisfactory at ultraviolet range. Near 320 nm, which is the peak of the emission spectrum of pure CsI scintillator, the quantum efficiency is about 30% and is not guaranteed by Hamamatsu. However, in the visible range, the quantum efficiency reaches 85% , which inspires the application of wavelength shifter in chapter 5.

APD is a dominant source of the temperature variations of the signal from the counter. To provide stable ECL response these variations are to be compensated. Thus, we measured the dependence of Hamamatsu APD's dark current

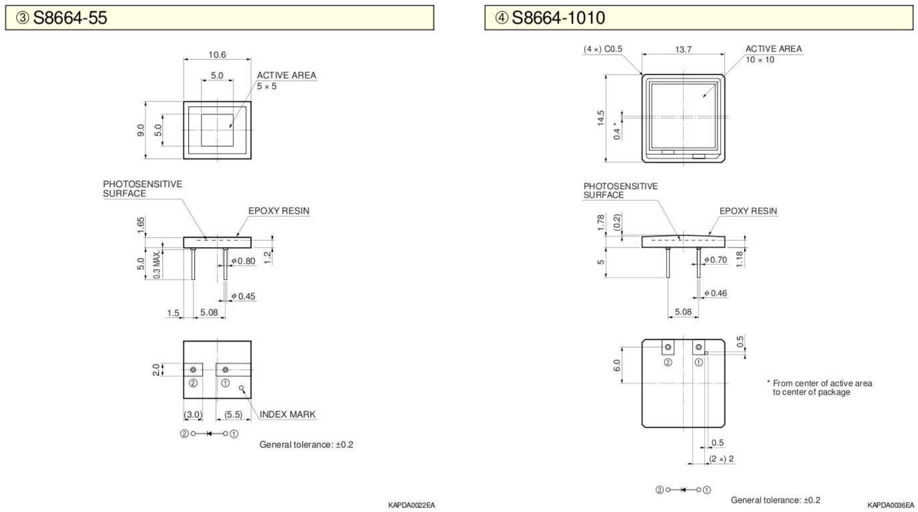

Figure 2.4: Diagram of the structure of APD [3].

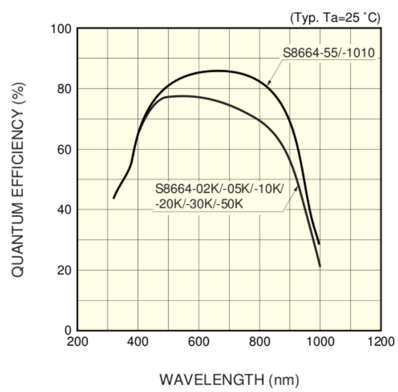

Figure 2.5: Quantum efficiency of APD versus wavelength [3].

and gain on temperature in the range from 10 °C to 43 °C (see Fig. 2.6 and 2.7).

At the operating point (under the bias voltage that gives APD gain = 50 at room temperature), the dark current of S8664-55 APD varies from 1 nA to 8 nA, and that of S8664-1010 APD varies from 1 nA to 30 nA. This low dark current is one of the advantages of APD that we mentioned before.

Relative temperature gain variations for S8664-55 and S8664-1010 APD's are shown in Table 4.1. A temperature compensation circuit in the bias voltage supply for APD is needed for the sake of the stability of the counter.

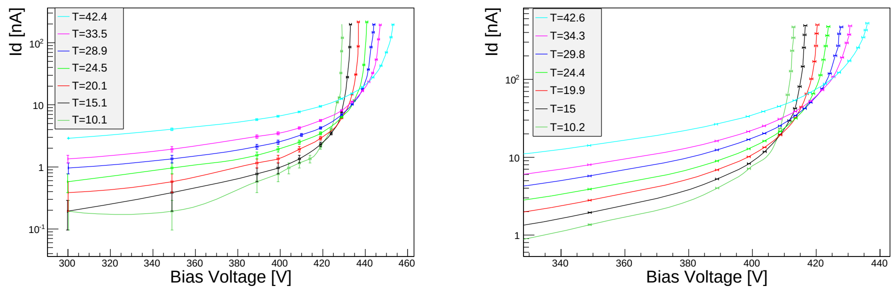

(a) S8664-55 (b) S8664-1010

Figure 2.6: The dependence of APD's dark current on temperature.

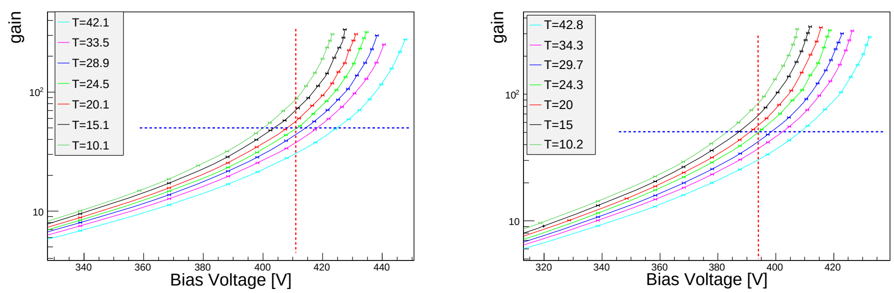

(a) S8664-55 (b) S8664-1010

Figure 2.7: The dependence of APD's dark current on temperature. The blue dashed line indicates gain=50. The red line dashed indicates the bias voltage which gives gain=50 at room temperature.

Table 2.1: Relative temperature gain variation, $(1/G)(dG/dT)$ (%/°C), for Hamamatsu S8664-55 and S8664-1010 APDs at different operating points with gain of 30, 50 and 100.

	APD gain		
APD type	30	50	100
S8664-55	-2.4 ± 0.1	-3.3 ± 0.1	-5.0 ± 0.2
S8664-1010	-2.3 ± 0.1	-3.1 ± 0.1	-4.9 ± 0.2

2.3 CAEN preamplifier

Figure 2.8: Picture of CAEN A1422B045F3 preamplifier [4].

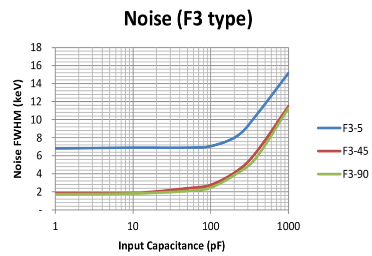

Figure 2.9: Noise of CAEN A1422 preamplifier versus input capacitance, provided by Hamamatsu [4]. The red line is our preamplifier A1422B045F3.

The CAEN A1422 preamplifer is a charge sensitive one, with 1, 4 or 8 channels available. In this measurement, a preamplifier of 4 channels (CAEN A1422B045F3) is employed (see Fig.2.8). And one test channel is also provided by the A1422. Both positive and negative input pulses are acceptable for A1422. The charge sensitivity is 45 mV/MeV (Si). The working conditions, up to 2000 V bias voltage and up to 1000 pF capacitance, are allowed at detection channels. The calibration capacitor in the test channel of the preamplifier used in our current counter system is measured to be 0.82 ± 0.05pF (see in Appendix).

Considering the case that S8664-1010 APD is attached to the detection channel, at capacitance 270 pF, the noise is 5 keV (see Fig.2.9). Indeed, it is low enough for the current requirement.

2.4 Shaping amplifier

Figure 2.10: Picture of CP-4467A shaping amplifier.

Figure 2.11: Picture of Hoshin C008 ADC [5]

Clear-Pulse 4467A is a CR-4RC fast filter amplifier (see Fig.2.10). Five options of shaping time are available, 20 ns, 50 ns, 100 ns, 200 ns and 500 ns. Coarse gain of the shaper ranges from 2 to 100. In addition, a fine gain from 1 to 3 is also provided.

2.5 ADC

Hoshin 16ch PHADC CAMAC C008 is employed in the system (see Fig.2.11). All 16 input channels are able to work at the same time, accepting both positive and negative input signals within absolute voltage amplitude 2.5 V. The amplitude of the input voltage signal is digitized by 12 bits.

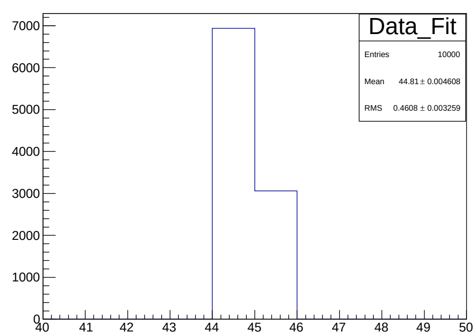

Figure 2.12: Histogram of the pedestal of C008 ADC. Full scale of x axis is 4096 channels.

The narrow pedestal distribution of the Hoshin ADC, only two channels out of 4096 channels (see Fig.2.12), shows high quality of the ADC.

Chapter 3

Study of equivalent noise charge

Suppression of electronic noise is crucial for the scheme with pure CsI and APD. In this chapter, the equivalent noise charge (ENC) of the readout electronic channel is measured to understand whether the correlated noise is well suppressed or not. First, a formula 3.2 is introduced to study ENC. All components in it have been experimentally measured. Then, the formula reveals a dependence of noise on shaping time as a means of finding the optimal noise in the unit of electron number. In addition, the real noise of HAMAMATSU S8664-55 APD and HAMAMATSU S8664-1010 APD are measured with shaping time ranging from 20 ns to 500 ns to verify the formula 3.2. Finally, based on the ENC, estimation of equivalent noise energy is made.

3.1 Noise analysis

The noise of the readout electronics has already been studied very well. Here the formula of the noise of a spectrometric channel without effect of internal amplification is directly quoted [6] without derivation.

$$Q_{noise}^2 = (2|e|I_d + \frac{4k_bT}{R_b} + i_{na}^2)K_iT_s + (4k_bTR_s + e_{na}^2)K_\nu\frac{C^2}{T_s} + K_{\nu f}A_fC^2, \quad (3.1)$$

where, e indicates the elementary charge of the electron, I_d the sensor bias current, k_b Boltzmann constant, T temperature, R_b the resistance of bias resistor, R_s the resistance of series resistor, C capacitance of sensor at detection channel, K_i, K_ν and $K_{\nu f}$ the factors depending on the shape of the signal from the shaping amplifier, A_f 1/f noise coefficient, T_s a characteristic time of shaper, i_{na}^2 and e_{na}^2 the noise of the amplifier.

In the case of APD, I_d can be regarded as dark current, at the order of nano-Ampere. The bias resistor $R_b = 120$ MΩ in our scheme, thereby this term can be neglected. K_i, K_ν and $K_{\nu f}$ can be calculated by the impulse response of the shaper [6]. In the case of CR-4RC shaper, theoretically, $K_i = 0.45$, $K_\nu = 1$, $T_s = 4 \times \tau(\textit{shaping time})$. In order to simplify the equation, $K_{\nu f}$ and A_f are combined together and expressed as E^2, stemming from the 1/f noise.

$4k_bTR_sK_\nu$, is expressed as B^2, stemming from the thermal noise. Taking into account amplification of the signal and avalanche fluctuation in APD, the first term, shot noise, now includes two new factor, g, gain of APD and F, excess noise factor. Adding i_{na}^2 and e_{na}^2 together, along with the additional noise from other components of the readout electronics such as shaper, ADC, wires, discriminator and computer, note as D^2. Omitting the subscript of K_i and Q_{noise}^2, the former equation can be written in the form:

$$Q^2 = \frac{2\ I_d\ K\ g\ F\ \tau}{e} + (\frac{B^2}{\tau} + E^2)C^2 + D^2. \tag{3.2}$$

ENC Q^2 now is in the unit of eletron number. This equation 3.2 will be frequently used throughout this thesis. And in next chapter, these parameters, B, E, D, K and F will be measured instead of those in 3.1.

3.2 Demonstration of the measurement of ENC

In order to measure the ENC, calibration signals, pulses of 50 mV in amplitude, 100 Hz in frequency and 50 μs of duration time, from a wave generator are sent to the test channel of preamplifier CAEN A1422B045F3. The pulses go through the preamplifier, then shaping amplifier, finally are read out by an ADC. A histogram of the output from ADC is made whose distribution is in a Gaussian distribution and the root mean square (RMS) is a measure of the noise.

In the case of measuring D, as portrayed in Figure 3.1, nothing is attached to the detection channel of the preamplier. So the formula 3.2 is simplified into $Q^2 = D^2$.

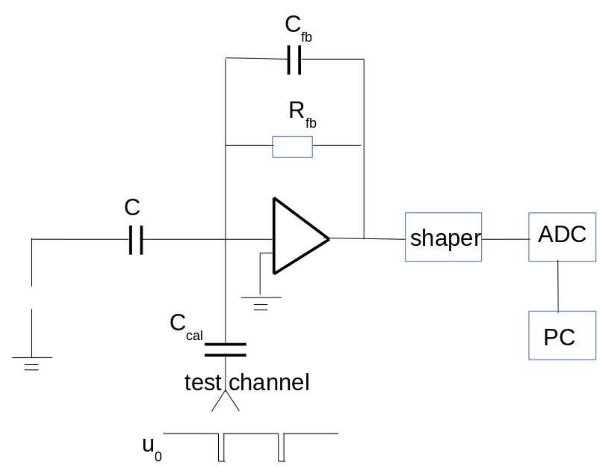

Figure 3.1: Scheme of measuring D. As nothing is attached at the detection channel during measurement,the shot noise and thermal noise related to the sensor at detection channel vanish.

Sending calibration signals of constant amplitudes in voltage to the test channel of preamplifer, after the pulses getting processed by the readout electronics chain, a Gaussian distribution (with mean value M and RMS σ) is obtained. Thereby $D = \frac{\sigma \cdot C_{cal} \cdot u}{M \cdot e}$ where C_{cal} indicates the capacitance of the calibration capacitor, u the amplitude of pulses in voltage and e the elementary charge.

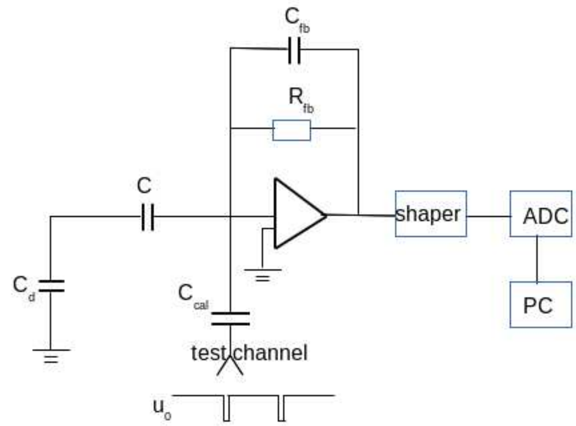

Figure 3.2: Scheme of measuring B and E. C_d indicates the capacitor attaching at the detection channel of preamplifier.

As for B (thermal noise coefficient) and E (1/f noise coefficient), two well measured capacitors are attached at the detection channel of preamplifier alternatively, as showed in Figure 3.2. Meanwhile, the calibration signals' amplitudes remain unchanged. When one capacitor is attached at the detection channel, the thermal noise term is introduced, $Q^2 = (\frac{B^2}{\tau} + E^2) \cdot C_d^2 + D^2$. C_d^2 stands for the capacitance of the capacitor at detection channel and τ for the shaping time. Through the usage of the first well measured capacitor C_1, a set of value of $\frac{B^2}{\tau} + E^2 = \frac{Q^2 - D^2}{C_1^2}$ is obtained. Here total noise $Q = \frac{\sigma \cdot C_{cal} \cdot u}{M \cdot e}$ is similar to the situation of measuring D, only the value of the mean and RMS differ. Changing the capacitor to C_2, a new set of value of $\frac{B^2}{\tau} + E^2 = \frac{Q^2 - D^2}{C_2^2}$ is obtained again. Then B and E can be obtained separately by fitting these two sets of values.

When it comes to K (shaper factor), a PIN-photodiode under proper biased voltage is operated at the detection channel of the preamplifier (see Fig 3.3). As PIN-photodiodes do not have internal amplification, there is no effect of excess noise F. At the same time, an LED is used, working as a source of light to irradiate the PIN-photodiode. So the shot noise term related with the current (see Eq 3.2) is introduced. The shot noise is measured as a function of photo current when the LED is turning on, which can extract the value of K.

While the LED is irradiating, the noise $Q^2_{with\ Iphoto} = 2\ e\ (I_d + I_{photo})\tau\ K + (\frac{B^2}{\tau} + E^2)C_d^2 + D^2$, where I_d is the dark current of PIN-photodiode and I_{photo} is the photo-electron current. When the LED is turned off, the noise can be expressed in $Q^2_{no\ Iphoto} = 2\ e\ I_d\ \tau\ K + (\frac{B^2}{\tau} + E^2)C_d^2 + D^2$. Therefore, it is obtained that $K = \frac{Q^2_{with\ Iphoto} - Q^2_{no\ Iphoto}}{2\ e\ I_{photo}\ \tau}$.

The situation is similar to the excess noise factor F (see Fig 3.4), instead of PIN-photodiode, this time an APD is attaching to the detection channel due to the fact that F is an important parameter of the APD itself originating from

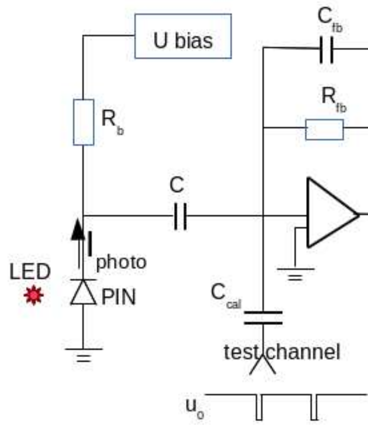

Figure 3.3: Scheme of measuring K. LED and bias voltage supply are employed in the scheme.

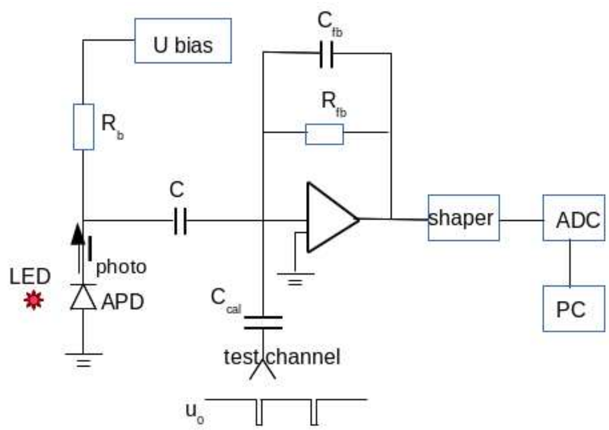

Figure 3.4: Scheme to measure F.

the flctuation of avalanche processes. Both K and F hold physics meaning, so they are measured separately. Apparently, $F = \frac{Q^2_{with\ Iphoto} - Q^2_{no\ Iphoto}}{2\ e\ I_{photo}\ \tau\ K\ g}$, where g indicates the gain of the APD under bias voltage.

3.3 Result of measurement

3.3.1 Additional noise, D

The result of the measurement of D is illustrated in the figure 3.5. D varies strongly with respect to shaping time. The origin of D noise is mainly from the shaping amplifier. Thus, there exists scope to reduce this factor by the replacement of CP-4467A to other type of shaper of better quality (ORTEC shaper, with shaping time 500 ns - 3 us was used to measure D. And we did confirm that better shaper provides smaller D. At shaping time 500 ns, the

D measured with ORTEC is only half of that of CP-4467A). In fact, this D factor is one of the most dominant terms in the total ENC of counter with APD compared with the value of total noise shown at the end of this section (see Fig 3.10).

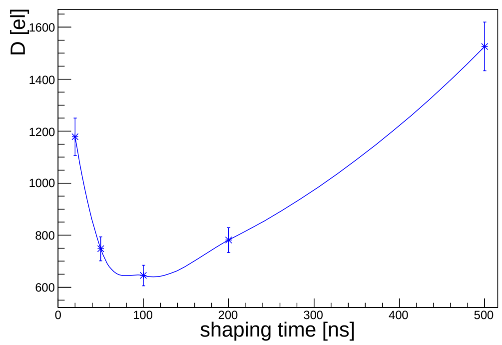

Figure 3.5: The measurement result of D versus shaping time in unit of electron numbers.

3.3.2 Thermal noise coefficient B and 1/f noise coefficient E

Two capacitors, of capacitance $C_1 = 96.4\ pF$ and $C_2 = 217.7\ pF$, with uncertainty 5% are used.

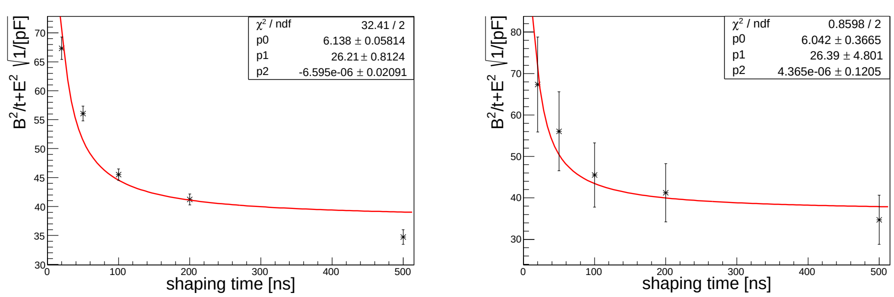

(a) without systematic error (b) with systematic error

Figure 3.6: The fitting result of B and E.

The fitting function is composed of $a + \frac{b}{x} + c \cdot x$, where a, b and c are free parameters to fit (notice that a term proportional to capacitance is also included in this function). It is showed by the figure 3.6 that the third term is negligible (as it should be) and it can be extracted that $B = 26.21 \pm 0.8124 \pm 4.801\ \frac{\sqrt{ns}}{pF}$ and $E = 6.138 \pm 0.0581 \pm 0.3665\ \frac{1}{pF}$. The systematic error is originated from the uncertainty of the capacitor attaching at the detection channel and the calibration capacitor inside the preamplifer.

3.3.3 Shaper factor, K

The shaper factor K is related to the shaper only. According to different shapers, the value changes. Here the result of CP-4467A is presented (see Fig 3.7), measured at shaping time 500 nanoseconds.

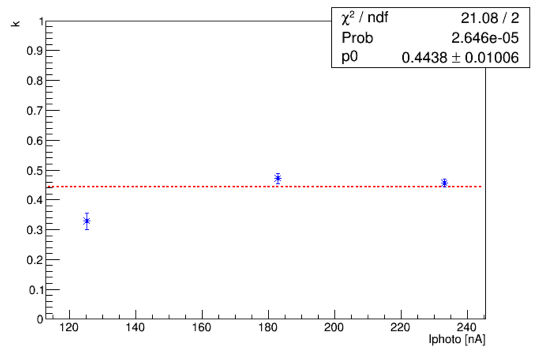

Figure 3.7: The measurement result of K of CP-4467A shaper.

In the situation of Belle II ECL, the intensity of photo current of APD reading out a pure CsI crystal will be mostly in the range from 40 to 100 nA. However, due to the shot noise's proportionality to the product of shaping time and current, it is difficult to measure the K factor accurately at small photo current. Therefore, the value measured at small photo current has large uncertainty. So, in this measurement, the range of I_{photo} is extended to 250 nA in order to measure the K factor properly. As a result, the average measured value agrees with the theoretical value (0.45 for CR-4RC shapers) very well, within 5 % error.

3.3.4 Excess noise factor, F

The excess noise factor of S8664-55 and S8664-1010 APD are presented respectively. At gain=50, $F = 5.1 \pm 0.5$ for S8664-55; $F = 3.4 \pm 0.4$ for S8664-1010 (see Fig 3.8).

At low bias voltage, the excess noise factor is supposed to be 1 due to the small avalanche, as it is stemming from the avalanche fluctuation. However, under low bias voltage the capacitance of APD S8664-1010 is lager than 400 pF which is the upper limit for preamplifier to work properly. Thereby a deviation occurs at 50 V in the Figure 3.8(b).

The relation of gain between bias voltage is a crucial property of APD, therefore it is also illustrated in Figure 3.9. The operating point gain=50 is reached when the bias voltage is approaching to 395V.

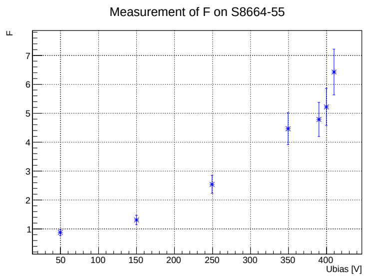

(a) F of S8664-55

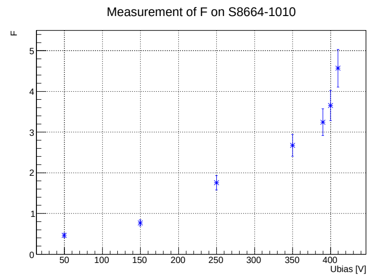

(b) F of S8664-1010

Figure 3.8: The measurement result of F versus bias voltage.

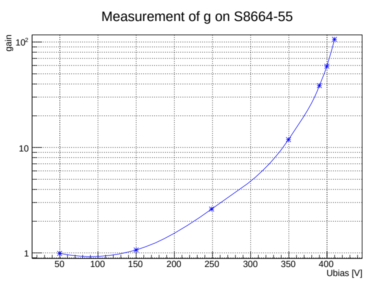

(a) gain of S8664-55

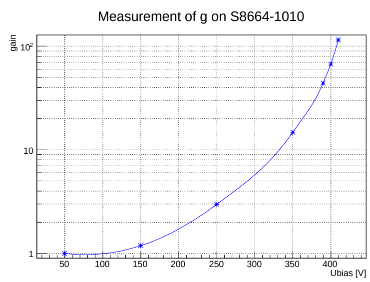

(b) gain of S8664-1010

Figure 3.9: The measurement result of gain versus bias voltage.

3.3.5 Total noise by Hamamatsu APD

The relation between noise and shaping time is illustrated in Figure 3.10. In the case of HAMAMATSU S8664-55 APD, the optimal noise is about 1050 electrons at the shaping time slightly below 100 nanoseconds. As for HAMAMATSU S8664-1010 APD, the optimal noise is much higher, about 1850 electrons at the shaping time around 100 nanoseconds.

As all components in the formula 3.2 are specifically measured (such as I_d, g, F, K, B and E), the total noise's dependence on the shaping time could also be verified by the sum of the result calculated by these components in the right side of the formula 3.2. Due to the complexity of the D factor, in order to simplify the situation, the D^2 on the right hand side of equation is moved to the left hand side. In other word, the formula is transformed into $Q^2 - D^2 = 2 \times e \times I_d \times \tau \times K \times g \times F + (\frac{B^2}{\tau} + E^2) \times C_d^2$. In this way, the measured total noise subtracting D factor in quadrature is verified by the calculated results of shot noise and thermal noise. Under the proper bias voltage which gives gain=50, in the case of S8664-55 APD, HAMAMATSU measures the dark current as 2 nA, capacitance as 80 pF. Combined with the results above, $B = 26.21, E = 6.138, K = 0.4438$ and $F = 5$, sum of shot noise and thermal noise is calculated. For S8664-1010 APD, HAMAMATSU measures the dark current as 8 nA and capacitance as 270 pF. $F = 3.4$. B, E and K remain

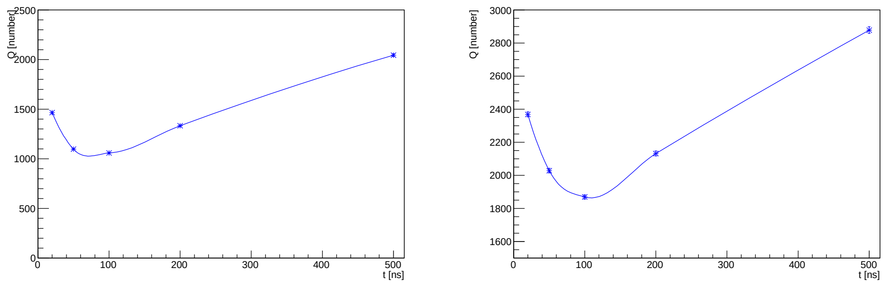

(a) total noise with S8664-55

(b) total noise with S8664-1010

Figure 3.10: The measurement result of total noise versus shaping time.

the same as they are not related to the APD.

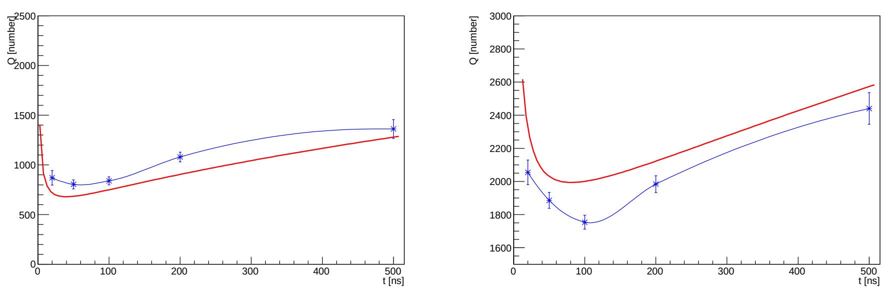

(a) S8664-55

(b) S8664-1010

Figure 3.11: The comparison between measured noise (blue line) and calculated result (red line). Measured noise is the measured results of total ENC subtracting D factor in quadrature. Using the measured result of I_d, g, F, K, B and E, the shot noise and thermal noise are calculated explicitly and illustrated by the red line.

The calculated sum of shot noise and thermal noise agrees with the measured result (see Fig. 3.11), especially in the case of S8664-55 APD. Thereby, we can conlude that this formula describes our shceme very well and uncorrelated noise is suppressed to a great extent. Regarding S8664-1010 APD, previous work [7]-[8] show that there is a large deviation about the capacitance of S8664-1010 APD from the average value 270 pF. The capacitance of the S8664-1010 APD measured at operating bias voltage in [7] is around 160 pF, and $233 \pm 7 \pm 11$ pF in [8]. Therefore, taking the value as 270 pF, granted by HAMAMATSU, does uplift the calculated line and explain the discrepancy very well.

3.4 Estimation of ENE

The measurement of ENC demonstrates the noise in the unit of electron numbers. In the real physical progress, the high energy particle deposits energy in the scintillator crystal. Then, the scintillator emits thousands of photons. Some of those photons hit the sensor, APD in our case, trigger an avalanche process and provide a large amount of electrons. Depending on the dimension of crystal, the light collection coefficient was simulated [see in Appendix 7.4], by which, the unit of noise in number of electrons can be turned into energy.

$$ENE = ENC/\alpha \tag{3.3}$$

And $\alpha = N_0 \times a \times QE \times g$, where N_0 indicates the number of photons emitted per MeV of deposited energy, a, light collection coefficient, suggesting the fraction of photons that can hit the sensor, QE and g, quantum efficiency and gain of APD respectively. In the case of the pure CsI crystals used in Belle II, $N_0 = 5000$ [9]. The light collection coefficient is simulated and found to be 0.016 for the counter with one S8664-1010 APD, and 0.004 for the counter with one S8664-55 APD. $QE = 0.3$ and $g = 50$ as explained before.

S8664-1010

$$ENE = \frac{1850}{5000(/MeV) \times 0.016 \times 0.3 \times 50} \approx 1.6MeV \tag{3.4}$$

S8664-55

$$ENE = \frac{1050}{5000(/MeV) \times 0.004 \times 0.3 \times 50} \approx 3.5MeV \tag{3.5}$$

Furthermore, if two APD's are attached to one crystal, the equivalent noise energy can be reduced by a factor of $\sqrt{2}$.

3.5 Discussion

In this chapter, it is obtained that the best noise level is achieved around shaping time 100 nanoseconds. This result matches the need of Belle II very well, where shaping time was 1 μs and pile up noise would be a tricky situation with such a shaping time, unless we reduce shaping time substantially. However, as the shaping time is targeted to be 30 ns, it is still needed to optimize the readout electronics in order to shift the lowest noise from shaping time 100 ns to 30 ns. Furthermore, by the measurement of equivalent noise charge, it is demonstrated that in order to suppress the total noise, the reduction on capacitance of the APD and improvement of shaper are the main ways to solution. In fact, compared with photopentodes and PIN-photodiodes, the capacitance of APD indeed is its distinct disadvantage. However, the high gain of APD showed in Figure 3.9, also makes up to the low light yield of the pure CsI scintillator.

Chapter 4

Measurement of equivalent noise energy

In this chapter, the measurement of equivalent noise energy (ENE) of the counter is presented. To reduce the ENE of the counter, 2 or 4 APD's are attached per crystal. First the detail of the pure CsI crystal will be explained. Then, the method of the equivalent noise energy (ENE) measurement will be explained, followed by the result of the measurement.

4.1 Pure CsI crystal

Figure 4.1: Photograph of the pure CsI crystal well wrapped.

The crystal used in this thesis is produced by Kharkov Company, Ukraine, of a truncated pyramidal shape. The front surface is 5 cm×5 cm, the backward surface 6 cm×6 cm and 30 cm in length (see Fig 4.1). This truncated pyramidal crystal was used in the Belle experiment. The crystal is wrapped by one layer of Gore-Tex teflon of 200 μm thickness and placed in a 40-μm aluminized mylar envelope. Optical grease OKEN-6262A is used to couple the APD to the crystal.

4.2 Demonstration of ENE measurement

When the cosmic mouns pass through and interact with scintillator, they deposite part of their energy in the scintillator which generates the scintillation light. Although it is a stochastic process how the cosmic mouns passing through the scintillator, there is a most probable energy that cosmic mouns deposite. A simulation of deposited energy of the cosmic muons in our crystal

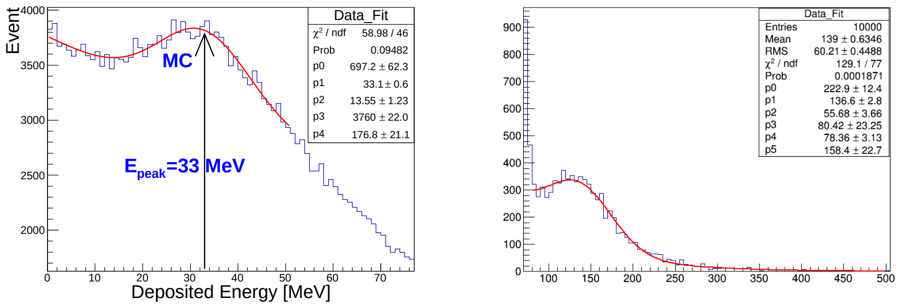

(a) Deposited energy spectrum

(b) Histogram from experiment

Figure 4.2: The peak position in the left figure is the most probable energy deposition in the Monte Carlo simulation of the deposited energy of cosmic muons in a pure CsI crystal. The histogram in the right figure is the data from experiment.

was developed, and the most probable energy deposition (position of the cosmic peak) was found to be about 33 MeV (see Fig.4.2 (a)). The algorithm of this Monte Carlo simulation is in the appendix. When we use cosmic muons to calibrate the scintillator experimentally, a spectrum of data is obtained (see Fig.4.2 (b)), whose peak position corresponds to the 33 MeV given by the simulation. Dividing 33 MeV by the channel number of the peak position of data, a parameter, *the conversion of ADC*, is obtained in the unit of [MeV/channel number]. Thus, when the calibration pulses are sent to the test channel of preamplifier (see Fig.3.4), the noise, again obtained by the RMS of the readout of ADC, now is converted into the unit of energy (MeV) by the usage of *the conversion of ADC* and named equivalent noise energy.

4.3 Results of ENE

In this section, the ENE of the counter with one APD per crystal is presented. Then the result of the counter with two S8664-1010 is presented to demonstrate the resulting improvement. After that, the effect of reflector wrapping on the crystal is studied. Finally the result of 4 APD's is presented. Accuracy of the measurement is limited by the relative temperature gain variation ($\frac{1}{G} * \frac{dG}{dT}$), accuracy of simulation of cosmic peak position and statistical accuracy of the data.

Counter with one APD

While attaching one APD to crystal, as shown by the figure 4.3, the best noise level occurs at 100 nanoseconds, 1.85±0.19 MeV for the ENE of the counter with one S8664-1010 APD and 2.71±0.27 MeV for that with one S8664-55 APD. This preliminary result is far away from the goal. Thereby several operations have been processed and stated below.

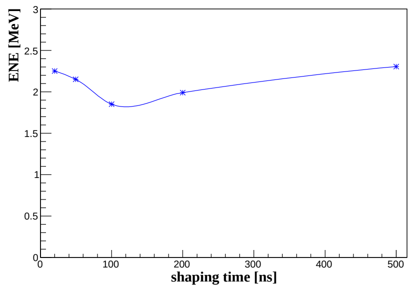

(a) S8664-1010

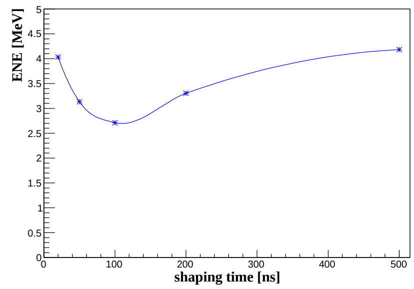

(b) S8664-55

Figure 4.3: The noise of Belle crystal versus shaping time. Blue line for total noise and black lines for APD noise.

Attaching two APD's per crystal

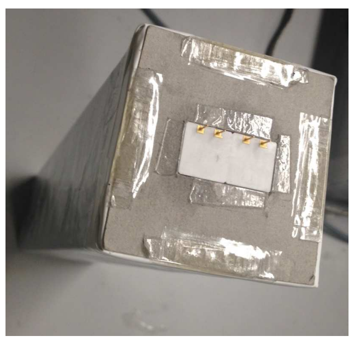

Figure 4.4: Photograph of attaching 2 APD's.

Attaching two APD's (see Fig. 4.4) can double the amount of collected scintillation light. As the noise is added in a quadratic way, the signal to noise ratio is improved by a factor $\sqrt{2}$. However, owing to discrepancy in the quality between these two S8664-1010 APD's, one APD is an old version and the noise of it is 1.2 times larger than that of the other one (due to its three times larger dark current), the noise is only suppressed by a factor 1.2, from 1.85 MeV to 1.56 ± 0.16 MeV (see Fig. 4.5).

Changing reflector

The Belle crystal was wrapped by a thin white teflon of thickness 75 μm. As thicker teflon owns a better reflectivity, and better reflectivity does help to increase the amount of the collected scintillation light, the effect of wrapping Belle crystal by thick white teflon of 200 μm is also studied. Indeed, a resulting improvement occurs. The noise gets reduced again from 1.56 MeV to 1.30 ± 0.13 MeV (see Fig. 4.6). A factor of 1.2 is earned on suppressing the noise. The

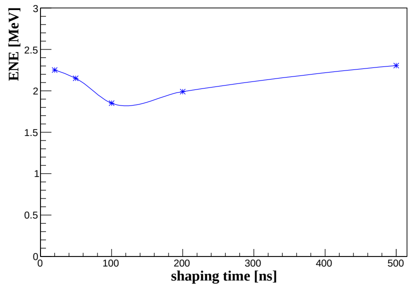

(a) 1 S8664-1010 APD

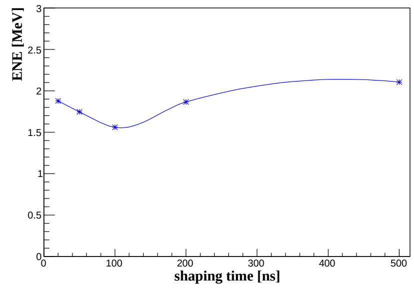

(b) 2 S8664-1010 APDs

Figure 4.5: ENE of the counter with 1 S8664-1010 APD and 2 S8664-1010 APD's

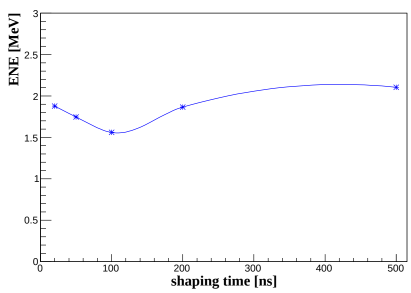

(a) thin teflon with 2 S8664-1010 APD

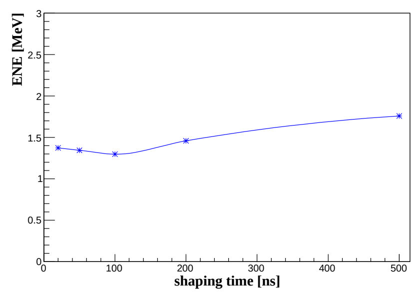

(b) thick teflon with 2 S8664-1010 APD

Figure 4.6: The difference between two reflectors.

study of the thickness of teflon is discussed in detail in next chapter, which states that 200 μm is thicker enough for our use.

In order to compare the noises of two types of APD, two S8664-55 APDs are also attached to crystal(see Fig. 4.7(b)). The noise 1.71 ± 0.17 MeV is higher than 1.30 ± 0.13 MeV of two S8664-1010 APDs. S8664-55's active area is only one fourth of S8664-1010, making it different to collect a huge amount of photons, resulting in a smaller signal, thereby the noise is higher.

Counter with four S8664-55 APD's

The ENE of the counter with four S8664-55 APD's has been measured (see Fig. 4.8). The ENE is reduced to 1.20 ± 0.12 MeV, earning a factor of $\sqrt{2}$ compared with the ENE of the counter with two S8664-55 APD's.

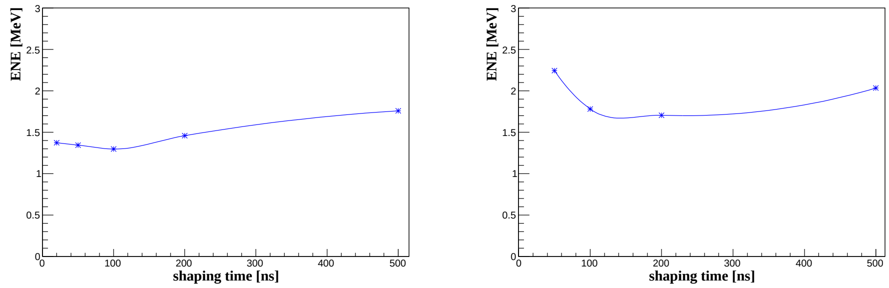

(a) two S8664-1010 APDs

(b) two S8664-55 APDs

Figure 4.7: S8664-1010 versus S8664-55

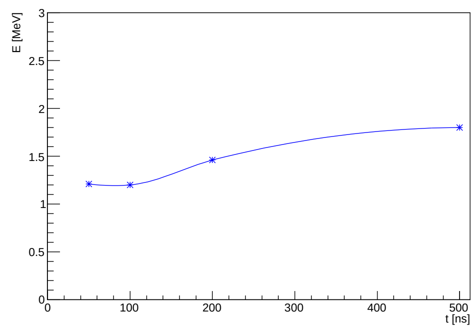

Figure 4.8: ENE of the counter with four S8664-55 APD's.

4.4 Discussion

Table 4.1: Minimal ENE can be obtained by counter with several APD's, in unit of [MeV]

APD number	ENE
2 S8664-1010	1.10 ± 0.11
2 S8664-55	1.71 ± 0.17
4 S8664-55	1.20 ± 0.12

Mainly the best noise level occurs at shaping time 100 nanoseconds, which agrees with the study in ENC method. And S8664-1010's performance is better than S8664-55 as the active area of S8664-1010 is larger than that of S8664-55. As stated above (also see table 4.1), if two S8664-1010 APD's of same quality are attaching to the crystal, the noise level is able to approach to 1.1 MeV. Furthermore, if four S8664-1010 APD's of same quality are attached, the situation can be improved to 0.8 MeV. As for S8664-55 APD, coupling with two

S8664-55 APD's gives ENE=1.71 ± 0.17, and 1.20 ± 0.12 MeV by four APD's. The achieved noise level hardly meets the required level. More effort is needed.

Chapter 5

Optimization to the final scheme

In the previous chapter, we obtain the ENE of the counter with several APDs. However, the achieved ENE is still quite far away from the required 0.5 MeV noise level. In this chapter, further studies have been done to suppress the ENE. As presented in chapter 3, the ENC of the counter has been suppressed very well. The only way to improve the ENE substantially is to increase the signal from APD. To increase the amount of the collected scintillation light, several studies were performed. Three optical greases, OKEN-6262A, BC-630 and TSF451-50M have been studied. The thickness of the reflector has been optimized. Also, the application of the wavelength shifter (WLS) is discussed in detail.

5.1 Optical greases

As the scintillation light of pure CsI crystal is in ultraviolet range (@320 nm), therefore the optical grease's performance in ultraviolet range is very critical. Signals of the counter consisting one S8664-1010 APD coupled with a pure CsI crystal by the optical greases OKEN-6262A, BC-630 and TSF451-50M alternatively have been measured with cosmic muons. The measured signal ratio is 1:0.95:0.85 (OKEN-6262A: BC-630: TSF451-50M). So, OKEN-6262A is kept to be used in the subsequent studies.

5.2 The thickness of teflon

In the previous studies [10], it was shown that the Gore-Tex teflon had the largest reflectivity even in the UV range (see Fig.5.1). The signal of the counter wrapped by teflon of one layer of 122 um, one layer of 185 um, two layers of 122 um and one layer of 500 um have been measured respectively. It was shown that 185 μm was thick enough, signals increasing no more than 5% with thicker teflon (see Fig. 5.2). And thicker wrapping material will aggravate the separation between the crystals in ECL, which induces the deterioration on energy resolution.

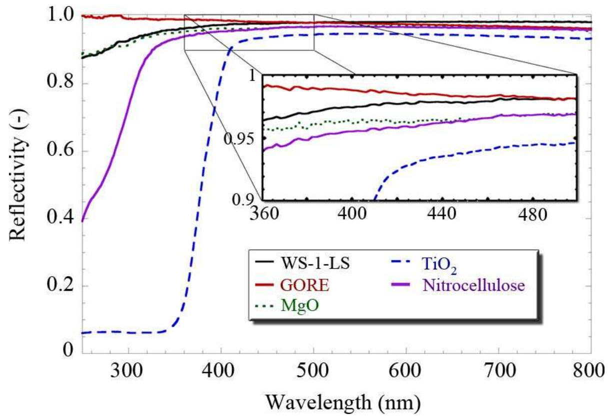

Figure 5.1: Reflectivity spectra for commonly used reflectors [10]

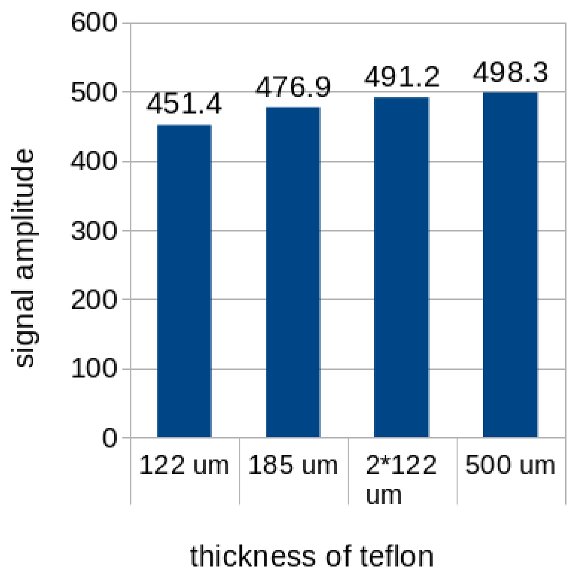

Figure 5.2: Signal amplitude of counter wrapped by teflon of different thickness

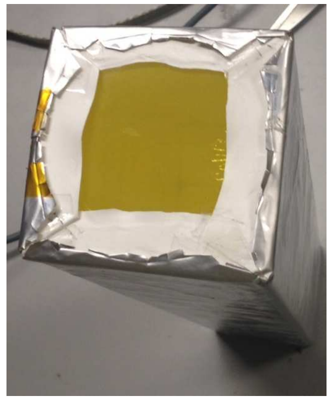

Figure 5.3: The WLS plate is attached to the crystal without optical grease. Then crystal and WLS plate are covered by teflon and aluminized mylar film.

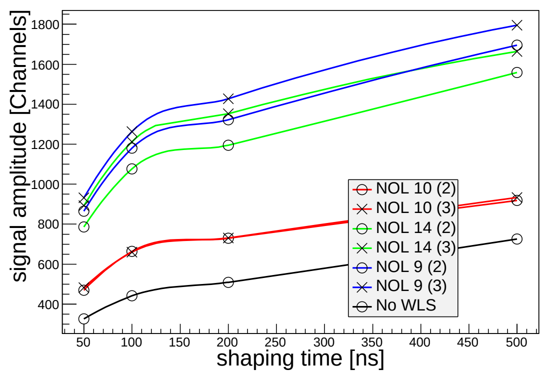

Figure 5.4: Signal amplitude of the counter coulpling with 2 S8664-1010 APD's. Three types of WLS plates have been applied. Number in parentheses indicates the optical density.

5.3 Wavelength shifting plates

The scintillation light of pure CsI is in ultraviolet range, where quantum efficiency of the APD is only about 30% and is not guaranteed by Hamamatsu. With wavelength shifting (WLS) plates containing nanostructured organosilicon luminophores (see Fig. 5.3), specially developed by LumInnoTech LLC [11], the ultraviolet scintillation light of pure CsI is shifted to the visible range where APD has maximal quantum efficiency of about 85% (see Fig. 2.5).

The WLS NOL9 provides the largest signal, earning a factor of 3 (see Fig.5.4). By this WLS, the ENE of counter coupling with 2 S8664-1010 was reduced to 0.53 ± 0.05 MeV and that of 4 S8664-55 to 0.45 ± 0.05 MeV (see Fig.5.5). The required noise level has been achieved.

Besides, recently, through the simulation of WLS (see Appendix) with three layers of progressively increasing refractive index, we obtained an enhancement of signal about 40% . The manufacture of WLS of this kind of structure is

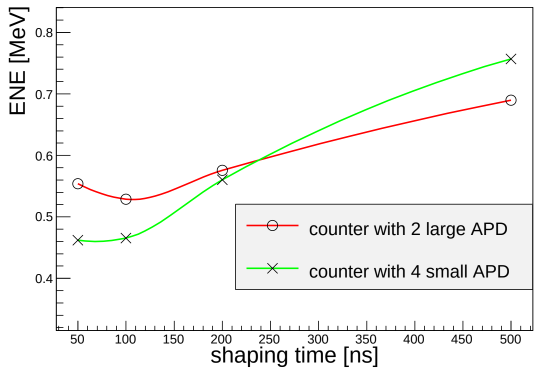

Figure 5.5: ENE of the counter consisting of WLS NOL 9 and two S8664-1010 APD's or four S8664-55 APD's. Here, in the counter of four S8664-55 APD, one APD is working at a gain much higher than 50, due to its operating bias voltage is lower than that of the other three S8664-55 APDs.

suggested to LumInnoTech LLC. If the techniques allows, we may test this kind of WLS in the near future.

Also, the investigation of radiation hardness of the WLS is on progress by our Italian colleagues in Belle II collaboration, which is very critical for the whole application.

Chapter 6

Conclusions and plans

Hamamatsu APD (S8664 type), a compact device that is insensitive to magnetic field and has a low dark current at Ubias = 400 V, provides a promising option for Belle II ECL end caps upgrade. Optimal wrapping material (Gore-Tex Teflon of 200 μm) and optical grease (OKEN-6262A) were established. WLS plates with innovative luminophores were applied to improve signal and earned a factor of about 3. Several APD's were used for the further suppression of equivalent noise energy. The ENE of the counter with 2 S8664-1010 APDs reaches to 0.53 ± 0.05 MeV and with 4 S8664-55 APDs reaches to 0.45 ± 0.05 MeV, which meet the project's requirement.

As mentioned at last chapter, the application of the WLS plate composed of layers with progressively increasing refractive index is worthwhile to be tested. Also, the specially developed shaper-FADC board for Belle II (with shaping time 30 ns) will be used in the measurement of ENE. By this board (shaping time 30 ns), we intend to achieve the current minimal noise. Besides, the scheme where APDs are mounted to the side edge of the thick WLS plate is also on the list.

Chapter 7

Appendix

7.1 How comes the goal 0.5 MeV on noise level.

Calorimeters measure the energy of the particle entering them by means of the absorption of the energy released by those particles. Electromagnetic showers are caused in the electromagnetic calorimeters, in usual case, scintillation crystals, specially used to detect energetic electrons and photons. Energy resolution of the electromagnetic calorimeter can be achieved to a good extent only when the shower is contained sufficiently. Energy resolution can be expressed by the formula:

$$\frac{\sigma_E}{E} = \sqrt{\left(\frac{1.9\%}{\sqrt[4]{E(GeV)}}\right)^2 + \left(\frac{A}{E(GeV)}\right)^2 + B^2}. \tag{7.1}$$

In real case, the dimension of the scintillation crystals is limited, which induces the shower leakage. And the resulting leakage fluctuations is the origin of the first term involving the fourth root of E. The second term stems from the electronics noise.

Taken into account the typical value of the energy of photon produced at Belle, 100 MeV, the first term gives an energy resolution 3.4%, in other words, $\Delta E = \sigma \approx 3.4$ MeV. The R&D of readout electronics is intended to suppress the electronics noise to the extent where leakage fluctuations is the only dominant part of the total noise. For that purpose, it's better that the electronics noise contributes the total noise less than 10 %. $\frac{\sigma^2_{E(ele)}}{3.4^2+\sigma^2_{E(ele)}} \leq 10\%$. therefore, $\sigma_{E(ele)} \approx 1.13$MeV. Empirically, at Belle, a shower involves five crystals. Thus for one crystal, $\sigma_{E(ele)} \approx \frac{1.13}{\sqrt{5}} \approx 0.5$MeV.

7.2 Measurement of the calibration capacitor in the preamplifier

In order to measure the value of the calibration capacitor, a capacitor with 2.2 nF is attached to the test channel, connecting with the calibration capacitor in series. As the value of calibration capacitor is only of the order 1 pF, the total capacitance is approximately equals to that of the additional capacitor, 2.2 nF. In terms of the comparison of the amplitude of the pulse after the preamplifier with additional capacitor and without it, the value of the calibration capacitance is obtained. The calibration capacitor was measured to be $C_{cal} = 0.82 \pm 0.05$pF.

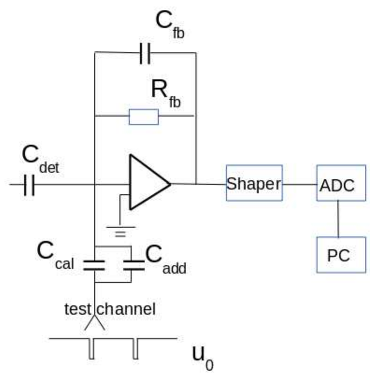

Figure 7.1: A capacitor C_{add} with well measured capacitance is added to the test channel in order to measure the capacitance of the calibration capacitor C_{cal}.

7.3 Simulation of the energy deposition of the cosmic muons

Here, the algorithm of the simulation of the energy deposition of the cosmic muons passing through a about 5.5 cm thick crystal is explained. This simulation gives the most probable energy deposition (peak position) of the cosmic muons.

1, a sphere containing the crystal (6cm × 6cm backward surface, 5cm × 5cm front surface, 30 cm in length) is built (see Fig.7.2).

2, The flux of cosmic muons is simulation based on the approximate extrapolation formula 7.2 from the Review of Particle Properties, available online at $http://pdg.lbl.gov$.

$$\frac{dN_\mu}{dE_\mu d\Omega} \approx \frac{0.14E_\mu^{-2.7}}{cm^2\ s\ sr\ GeV} \times \{\frac{1}{1+\frac{1.1E_\mu \cos\theta}{115\ GeV}} + \frac{0.054}{1+\frac{1.1E_\mu \cos\theta}{850\ GeV}}\}. \tag{7.2}$$

3, the event in which the muon penetrates two surfaces of the crystal is picked and the length of the path entering the crystal is calculated.

4, the deposited energy is calculated based on the Bethe equation 7.3.

$$\langle -\frac{dE}{dX}\rangle = Kz^2\frac{Z}{A}\frac{1}{\beta^2}\left[\frac{1}{2}ln\frac{2m_ec^2\beta^2\gamma^2W_{max}}{I^2} - \beta^2 - \frac{\delta(\beta\gamma)}{2}\right] \tag{7.3}$$

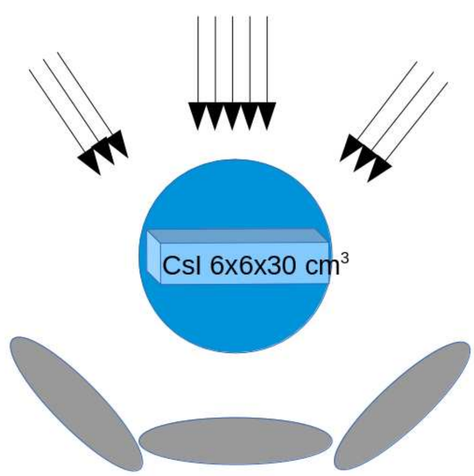

Figure 7.2: The merit of the sphere is that its projection to any angle is the circle of same size, which makes the application of flux formula 7.2 in an easy way. Also, in this simulation, crystal with any shape is allowed.

7.4 Simulation of light collection coefficient

Here, the algorithm of the simulation of light collection coefficient of the APD catching photons generated by crystal is explained.

1, photons are generated randomly and uniformly inside the crystal.

2, through the scalar product to the normal vectors of six surfaces, it can be determined whether the photon is inside of the crystal or not.

3, the photon propagates, When it reach the boundaries, reflection or absorption occurs. Specular reflection and diffuse reflection are both considered in the case when reflection occurs. When reaching the APD region, Fresnel equation is used to calculated to determine the ensuing step, whether to reflect or to penetrate.

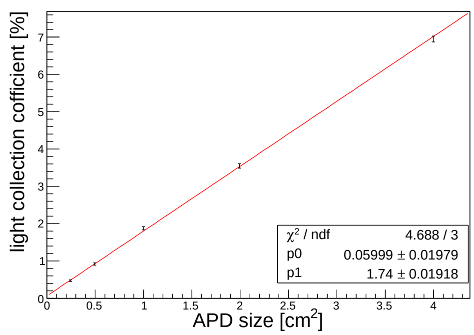

Figure 7.3: Result of the simulation: crystal (refractive index = 2) + optical grease (refractive index = 1.453) + APD (the glass window covering APD has refractive index = 1.5). It is assumed that the crystal is wrapped by the teflon with a reflectivity of 98%. The attenuation length of the pure CsI crystal is assumed to be 1.5 m.

7.5 Attaching WLS to crystal with/without optical grease

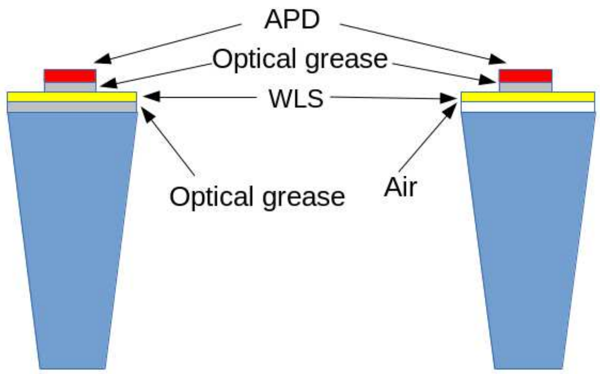

Figure 7.4: Demonstration of attaching the WLS to crystal.

The refractive index of the optical grease, pure CsI crystal and WLS are 1.453, 1.95 and 1.5 respectively. Therefore, without optical grease between crystal and WLS, the low index of air (n=1) increases the possibility of total reflection of WLS scintillation light. In other words, more amount of the photon emitted by the luminophore of WLS will propagate toward the APD side. This effect was measured and shown in Fig.7.5. A factor of 1.1 is achieved on the signal enhancement.

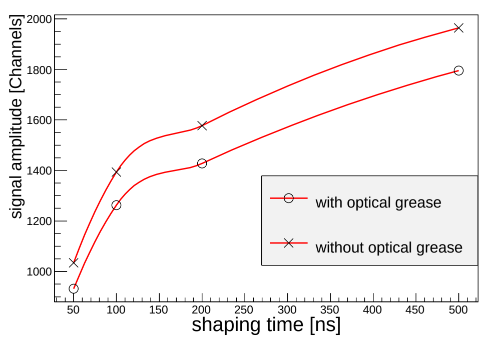

Figure 7.5: Signal amplitudes of the counter with 2 S8664-1010 APD's. Without optical grease between crystal and WLS, the signal is larger.

7.6 Simulation of progressively increasing refractive index

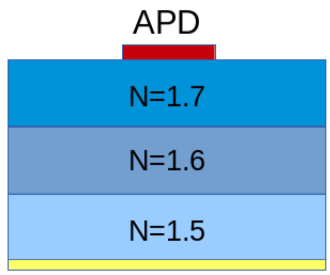

Figure 7.6: Demonstration of geomical structure.

This is simulation of WLS plates of layers with progressively increasing refractive index. The algorithm is similar to last section. Layers of progressively increasing refractive index functions as lens converging the light. A large area APD (S8664-1010) with sensitive area 1 cm^2 is attached to the 6x6 cm^2 WLS. The thickness of WLS is 5 mm. The photon is isotropically generated by the nanostructured organosilicon luminophores at the bottom, the yellow part in picture. It is assumed that the WLS is wrapped by teflon whose reflectivity is 98%, in lateral and at the top excluding APD part, and optical grease beneath the WLS. The simulation shows an enhancement of 1.48 $\pm$ 0.02.

Bibliography

[1] T.Abe, et al., Belle II technical design report, arXiv:1011.0352 [physics.ins-det].

[2] V.Aulchenko, et al., "Electromagnetic calorimeter for Belle II." Journal of Physics: Conference Series. Vol. 587. No. 1. IOP Publishing, 2015.

[3] www.hamamatsu.com/jp/en/index.html

[4] www.caen.it/csite/HomePage.jsp

[5] www.kagaku.com/hoshin/english.html

[6] H.Spieler, Analog and Digital Electronics for Detectors, Proceedings of the 2003 ICFA School on Instrumentation, Itacuruca, Brazil (2003).

[7] A.Hmelova, Avalanche Photodiode Investigation for Fast Scintillators, UTRIP Report (2012)

[8] Y. Jin, The measurement on capacitance by RC shape method, 2012 http://hep.phys.s.u-tokyo.ac.jp/ jin/CapacitanceMeasurement.pdf

[9] I.V.Bedny, et al., Study of the radiation hardness of the pure CsI crystals, Nucl. Instrum. Meth. A 598.1(2009) 273-274.

[10] M.Janecek, Reflectivity spectra for commonly used reflectors, IEEE Trans. Nucl. Sci. 59.3 (2012) 490-497.

[11] S.A.Ponomarenko, et al., Nanostructured organosilicon luminophores and their application in highly efficient plastic scintillators. Scientific reports 4 (2014).

Acknowledgements

I would like to express my gratitude first to Prof. Hiroaki Aihara and Dr. Denis Epifanov for their instruction that helped me complete this study which I regarded as an impossible mission two years ago. I am also grateful to everyone in this lab, Prof. Masashi Yokoyama, Dr. Yoshiyuki Onuki, Dr. Ian Watson, Kuniko Kono, Clement Ng, Nobuhiro Shimizu, Yusuke Suda, Taichiro Koga, Junya Sasaki, Hiroko Niikura, Naruhiro Chikuma, Fuminao Hosomi and Tianmeng Lou, for their helps in my study and daily life. Also, I would like to take this opportunity to express my sincere thanks to the Ministry of Education, Culture, Sports, Science and Technology of Japan for offering me the MEXT scholarship which covers my living expense and tuition fee here. Finally, I thank my parents for the unceasing encouragement and support.